AIAA JOURNAL
Vol. 45, No. 8, August 2007

Technical Notes

TECHNICAL NOTES are short manuscripts describing new developments or important results of a preliminary nature. These Notes should not exceed 2500 words (where a figure or table counts as 200 words). Following informal review by the Editors, they may be published within a few months of the date of receipt. Style requirements are the same as for regular contributions (see inside back cover).

High-Order Behaviors of Weighted Compact Fifth-Order Nonlinear Schemes

Liu Xin,* Deng Xiaogang,† and Mao Meiliang‡
China Aerodynamics Research and Development Center, 621000 Sichuan, People's Republic of China

DOI: 10.2514/1.23797

I. Introduction

THE typical theory for the finite difference method is that partial difference equations (PDEs) are discretized in space using a Taylor series expansion and solving it for the variables at discrete points. The derivatives are written as functions of variables on neighboring points. The approximations are said to be high-order accurate when the power p of the leading truncate error $O(h^p)$ is greater than two. Because of the advantages of high-flow structure resolution and nice discontinuity capturing precision, high-order accurate schemes are playing important roles in computational fluid dynamics (CFD).

Nonlinear high-order schemes for computing turbulence and aeroacoustic flows, which contain shock, have received more and more attention since the last decade. Although compact schemes have been derived by some researchers like Lele [1] and Gaitonde and Shang [2], they were poorly used in capturing the shock owing to their linear property in construction. Cockburn and Shu [3] proposed fourth-order compact nonlinear schemes based on a total variation diminishing (TVD) and total variation bounded (TVB) concept. Hu et al. [4] developed a fifth-order upwind compact scheme to solve the acoustic phenomena arising from shock-vortex interactions. According to the principles from the physical consideration, Zhang et al. [5] constructed a mixing method, which degenerated into the second-order nonoscillatory, containing no free parameters and dissipative (NND) scheme in the shock region and retained high-order accuracy elsewhere. An appropriate weight technique treated in high-order scheme construction may also differentiate the vortex in the smooth region and shocks robustly. Levy et al. [6] applied fourth-order central weighted essentially nonoscillatory (WENO) to hypersonic flows. Shu [7] used fifth-order WENO for shock problems.

Deng [8] and other researchers have developed a variety of compact high-order accurate schemes. A type of one-parameter linear dissipative compact scheme (DCS) was derived as to damp out the dispersive and parasite errors in the high-wave-number regions when central compact schemes were used. Although the linear compact schemes often caused numerical oscillations in the vicinity of discontinuities, a fourth-order cell-centered compact nonlinear finite difference scheme (CNS) [9] was then derived. An adaptive interpolation of variables at cell edges was designed, which automatically jumped to local one as discontinuities were encountered. It was a way to make the overall compact scheme capture discontinuities in a nonoscillatory manner. Afterward, using the weighted technique of Jiang and Shu [10] for interpolation at cell edge, fourth- and fifth-order weighted compact nonlinear schemes (WCNS) were developed [11,12]. They were more efficient than CNS, for two tridiagonal inversions were cancelled and no logical algorithms were needed. To eliminate the unphysical oscillations in the vortex field near the shock wave when inviscid flow was computed, Deng constructed high-order dissipative weighted compact nonlinear schemes (DWCNS) [13], which improved the ability of restraining nonphysical oscillation in the vorticity field. For viscous flow computations, as proposed in [13], WCNS-5 and WCNS-E-5 would better be used.

This Note shows the high-order features of WCNS including WCNS-E-5 and WCNS-5 with such typical high-order schemes as the explicit upwind biased fifth-order scheme (EUW-5) [14], Padé [1], and other special schemes like WENOs [6,7], and the explicit fifth-order shock-fitting upwind scheme [15]. We do the Fourier analysis to discuss WCNS-E-5 and WCNS-5 with EUW-5 and Padé. Owing to nontridiagonal inversion, WCNS-E-5 acts more efficiently than WCNS-5 during computations. Therefore, in Sec. IV, we use WCNS-E-5 to solve the multidimensional inviscid/viscous flows. WCNS-E-5 obtains several numerical results to show the good performances with those by WENOs and the explicit fifth-order shock-fitting upwind scheme.

II. Construction of Weighted Compact Fifth-Order Nonlinear Schemes

Let $U_i = U(\xi_i, t)$ $(\xi_i = ih)$ be the numerical solution of the hyperbolic conservation laws, at every node ξ_i, the model equation can be semidiscretized as

$$\left(\frac{\partial U}{\partial t}\right) = -E'_i \tag{1}$$

here E'_i represents the approximation to the spatial derivative. Based on the cell-centered finite difference compact schemes, E'_i can be computed as the following forms:

1) WCNS-5,

$$\frac{9}{62}E'_{i-1} + E'_i + \frac{9}{62}E'_{i+1} = \frac{63}{62h}(\tilde{E}_{i+1/2} - \tilde{E}_{i-1/2}) + \frac{17}{186h}(\tilde{E}_{i+3/2} - \tilde{E}_{i-3/2}) \tag{2}$$

2) WCNS-E-5,

$$E'_i = \frac{75}{64h}(\tilde{E}_{i+1/2} - \tilde{E}_{i-1/2}) - \frac{25}{384h}(\tilde{E}_{i+3/2} - \tilde{E}_{i-3/2}) + \frac{3}{640h}(\tilde{E}_{i+5/2} - \tilde{E}_{i-5/2}) \tag{3}$$

Received 29 April 2006; revision received 17 April 2007; accepted for publication 18 April 2007. Copyright © 2007 by the American Institute of Aeronautics and Astronautics, Inc. All rights reserved. Copies of this paper may be made for personal or internal use, on condition that the copier pay the $10.00 per-copy fee to the Copyright Clearance Center, Inc., 222 Rosewood Drive, Danvers, MA 01923; include the code 0001-1452/07 $10.00 in correspondence with the CCC.

*Associate Professor, High Speed Aerodynamics Institute; liuxing_76@sina.com.
†Professor, Computational Fluid Dynamics Institute; xgdeng@my-public.sc.cninfo.net. Member AIAA.
‡Professor, Computational Fluid Dynamics Institute; mml219@163.com.

In Eqs. (2) and (3), $\tilde{E}_{i\pm1/2} = E(\tilde{U}_{i\pm1/2})$ denotes the numerical flux at the cell edges. The weighted technique is used in the $\tilde{U}_{i\pm1/2}$ interpolations. The idea is that each of the chosen stencils is assigned a weight factor, which determines its contribution to the final approximation of the cell-edge value. The weights are designed in such a way that in the smooth region they approach the optimal weights to achieve fifth-order accuracy and require nontridiagonal inversion, whereas in the regions near the discontinuities, the weight of the stencil, which contains the discontinuities, is assigned nearly zero. Therefore the weighted interpolations are prevented from crossing discontinuities, whereafter the third-order interpolations are enforced in these regions. For more details, see, [11–13].

The boundary schemes have an important effect on the solution of the whole flowfield. As shown by Gustaffson [16], for a pth order interior scheme, the accuracy of the boundary schemes can be $(p-1)$th-order accurate without reducing the global accuracy of the interior scheme. For Eqs. (2) and (3), several boundary and near boundary schemes are derived in [12,13], in which more detailed discretization and interpolation of viscous flux for Navier–Stokes equations are also developed.

III. Fourier Analysis of Weighted Compact Fifth-Order Nonlinear Schemes

The dissipative and dispersive properties of WCNS by the Fourier analysis are further discussed in this section. Consider the semidiscrete form of the scaled linear hyperbolic equation

$$\frac{\partial u_i}{\partial t} + cu'_i = 0 \tag{4}$$

with a periodic function

$$u \equiv \exp(\mathrm{Im}\,\omega x) \tag{5}$$

where $c > 0$ is a constant speed. The difference error of first derivative is approximated by the comparison of the Fourier coefficients $(u'_k)_{\mathrm{fd}}$ with the exact u'_k. Defining the modified wave number $\omega^* = \omega^*_r + \mathrm{Im}\,\omega^*_i$, then Eq. (5) can be differenced as

$$(u')_{\mathrm{fd}} = \mathrm{Im}\,\omega^* u \tag{6}$$

The accurate solution of Eq. (4) with the initial condition of Eq. (5) can be obtained by substituting $u(x,t) = A(t)\exp(\mathrm{Im}\,\omega x)$ into Eq. (4)

$$u_i = \exp(c\omega^*_i t)\cdot\exp\left[\mathrm{Im}\,\omega\left(x_i - c\frac{\omega^*_r}{\omega}t\right)\right] \tag{7}$$

The cell-centered schemes for the u'_i have the form

$$\kappa u'_{i-1} + u'_i + \kappa u'_{i+1} = \frac{a}{h}(\tilde{u}_{i+1/2} - \tilde{u}_{i-1/2}) + \frac{b}{h}(\tilde{u}_{i+3/2} - \tilde{u}_{i-3/2}) + \frac{c}{h}(\tilde{u}_{i+5/2} - \tilde{u}_{i-5/2}) \tag{8}$$

Substituting Eqs. (5) and (6) into Eq. (8) and using the optimal interpolation

$$\tilde{u}_{i+1/2} = u_i + \frac{1}{128}(3u_{i-2} - 20u_{i-1} - 38u_i + 60u_{i+1} - 5u_{i+2})$$

we get the modified wave number function $\omega^* h = \omega^*(\omega h)h$.

Figure 1 shows the real and imaginary parts of $\omega^* h$ of WCNS-5 and WCNS-E-5 compared with EUW-5 and fourth-order Padé schemes. It can be observed that $\omega_i h < 0$ for all schemes but Padé (whose $\omega_i h$ equals zero), which just corresponds to the dissipative property. In terms of the modified wave numbers, WCNS-5 and WCNS-E-5 have almost the same dissipative and dispersive features as each other, and they both are superior to EUW-5.

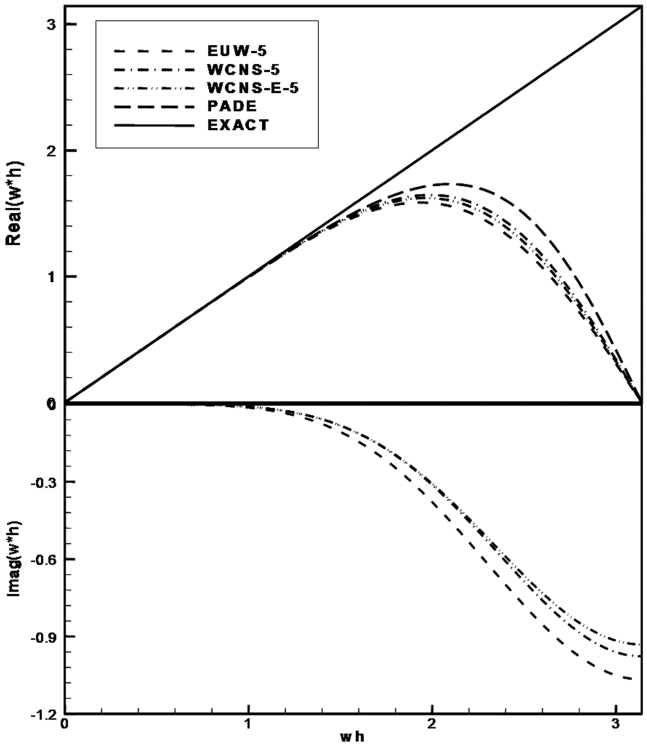

Fig. 1 Modified wave number of WCNS compared with EUW-5 and Padé.

Now define an error tolerance ε as

$$\left|\frac{\omega^*(\omega h)h - \omega h}{\omega h}\right| \le \varepsilon$$

Within the specified error tolerance, the range of well-resolved waves can be determined. We then use the fraction $e_1 \equiv \omega_f/\pi$ to represent as a measure of the resolving efficiency of a scheme, where ω_f is the shortest well-resolved wave. Table 1 shows the resolving efficiency of schemes for three different values of the error tolerance, i.e., $\varepsilon = 0.1, 0.01$, and 0.001. It is obvious that WCNS-5 and WCNS-E-5 have little difference from each other, and they stay close to the exact differentiation over a wider range of wave numbers than the other two schemes, when $\varepsilon = 0.01$ and 0.001.

In the multidimensional equation computation, the phase error is characterized by the form of anisotropic phase speed. The phase speeds of different wave numbers in a two-dimensional problem are shown as [1]

$$\omega^{**} = \frac{\omega^*(\omega h,\theta)h}{\omega h} = \frac{\cos\theta\omega^*(\omega h\cos\theta)h + \sin\theta\omega^*(\omega h\sin\theta)h}{\omega h}$$

where θ is the angle between the propagation direction and the axis. The anisotropy is displayed in Fig. 2 for the second-order center scheme, WCNS-5, WCNS-E-5, EUW-5, and Padé. The curves are plotted for

$$\frac{\omega h}{\pi} = \frac{1}{50}, \frac{5}{50}, \cdots, \frac{45}{50}, \frac{50}{50}$$

The outermost curves are circles corresponding to the small ωh. For these waves, the propagation is isotropic. The innermost curves

Table 1 Resolving efficiency of schemes

Scheme	$\varepsilon = 0.1$	$\varepsilon = 0.01$	$\varepsilon = 0.001$
EUW-5	0.545	0.355	0.235
WCNS-5	0.570	0.370	0.250
WCNS-E-5	0.560	0.365	0.245
Padé	0.595	0.360	0.205

a) 2nd-order scheme b) WCNS-5 c) WCNS-E-5 d) EUW-5 e) *Pade′*

Fig. 2 Curves of schemes' phase-speed anisotropy.

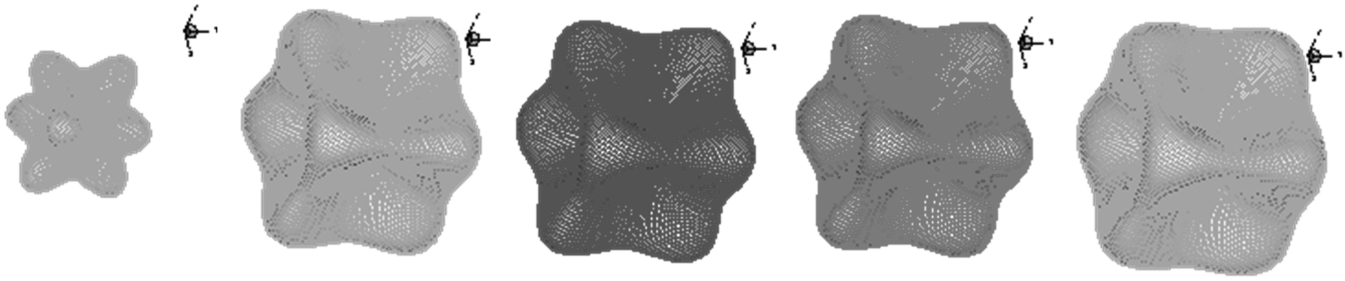

a) 2nd-order scheme b) WCNS-5 c) WCNS-E-5 d) EUW-5 e) *Pade′*

Fig. 3 Surface of schemes' phase-speed anisotropy.

correspond to the shortest waves resolved on the mesh. Among the schemes, the innermost curve of the second-order scheme is the smallest. The anisotropic features of the high-order schemes are little different from one another, and especially the behaviors of WCNS-5 are very close to those of WCNS-E-5.

For the three-dimensional phase speed, the following formula is derived as

$$\omega^{***} = \frac{\cos\theta\cos\varphi\omega^*(\omega h\cos\theta\cos\varphi)h + \cos\theta\sin\varphi\omega^*(\omega h\cos\theta\sin\varphi)h + \sin\theta\omega^*(\omega h\sin\theta)h}{\omega h}$$

Here θ is the angle between the propagation direction and the $x-y$ plane, and φ means the angle caused by the wave propagation in the $x-y$ plane with x axis. Subfigures in Fig. 3 show the anisotropic characteristics of the schemes when $\omega h = \pi$. Similar to those in two-dimensional flows, the resolved shorter waves propagate in the anisotropic way with the least error along ± 45 deg angles. The larger the surface configuration is, the narrower range of short wave the phase error is limited to.

By the Fourier analysis, the fifth-order WCNS (WCNS-E-5 and WCNS-5) behave as good as EUW-5 and Padé, and they act as almost the same characteristics as each other. However compared with WCNS-5, WCNS-E-5 requires nontridiagonal inversion during computation, which improves the computational efficiency. Therefore we apply WCNS-E-5 to the following complicated flows.

IV. Numerical Tests

Several transient flows are numerically simulated to compare WCNS-E-5 with WENOs [6,7] and the explicit fifth-order shock-fitting upwind scheme [15]. They are divided into two groups: inviscid flow and viscous flow. Roe's flux difference scheme [17] is used in the inviscid flow simulation and Steger–Warming vector flux splitting scheme [18] in the viscous flow simulation. The temporal term is discretized with the third-order TVD Runge–Kutta method [19].

Example 1. The two-dimensional Riemann problem for the Euler equations of gas dynamics is solved with the initial conditions shown in Fig. 4. In this computation, we simulate the results of interactions between different waves including rarefaction wave (from 2 to 1), shock wave (from 4 to 2), and contact surfaces (from 3 to 4 and from 3 to 1). We use the grid points of 200×200. Figure 5 shows the computed contours by WCNS-E-5 and those [6] by WENO when time equals 0.2. WENO with 400×400 indicates some oscillation within 2 and 4, whereas WCNS-E-5 does not. Furthermore WCNS-E-5 uses much fewer grids than WENO.

Example 2. The second example describes the interaction problem between a vortex and a stationary shock. It is a good model for sound waves that are generated when turbulence interacts with shock waves with shock structures in a jet plume resulting in broadband noise. The stationary Mach 1.1 shock is positioned at $x = 0.5$ and normal to the x axis. Its left state is $(\rho, u, v, p) = (1, M\sqrt{\gamma}, 0, 1)$. A small vortex

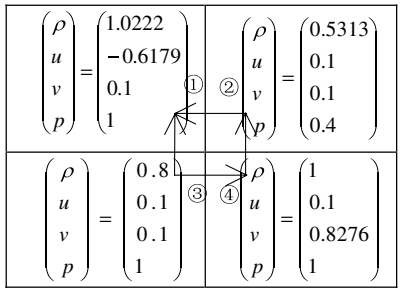

Fig. 4 Initial conditions for two-dimensional Riemann problem.

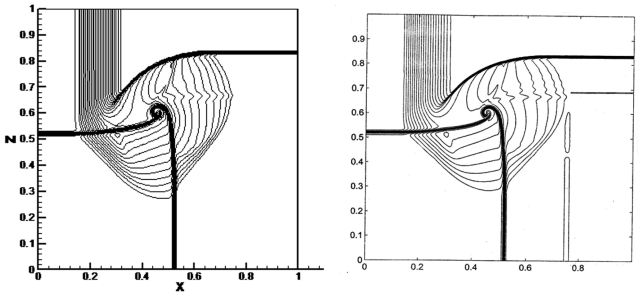

a) b)

Fig. 5 Density contours a) WCNS-E-5 with 200 × 200, and b) WENO with 400 × 400 [6].

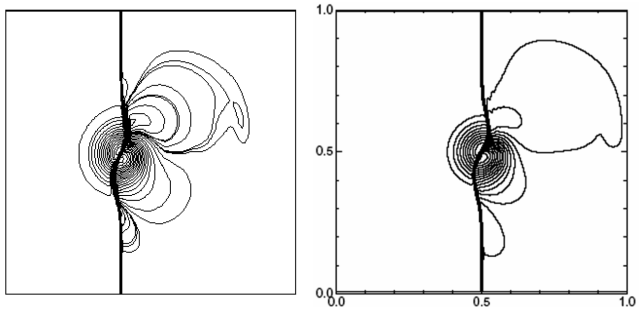

a) b)

Fig. 6 Pressure contours a) WCNS-E-5, and b) fifth-order WENO [7].

centers at $(x_c, y_c) = (0.25, 0.5)$ and is superposed to flow left to the shock. We describe the vortex as a perturbation to the velocity, temperature, and entropy of the mean flow and denote it by $(\delta u, \delta v) = \varepsilon \iota e^{\alpha(1-\iota^2)}(\sin\theta, -\cos\theta)$, $\delta T = -[(\gamma-1)\varepsilon^2/4\alpha\gamma]e^{2\alpha(1-\iota^2)}$, and $\delta S = 0$, where $\iota = r/r_c$ and $r^2 = (x-x_c)^2 + (y-y_c)^2$. Here ε indicates the strength of the vortex, α controls the decay rate of the vortex, and r_c is the critical radius for which the vortex has the maximum strength. In our test, we choose $\varepsilon = 0.35$, $\alpha = 0.204$, and $r_c = 0.05$. Figure 6 shows the results of the pressure contours at $t = 0.2$ by WCNS-E-5 and those [7] by Shu's WENO. When the vortex core passes through the shock, the bifurcation is being created, which causes shock to be split into two triple points connected with a Mach stem. That the vortex remains a well-defined circular shape shows the two fifth-order schemes have accurately represented the shock-vortex interaction, except for the small oscillation caused near the shock by WENO.

Example 3. We use WCNS-E-5 to study the hypersonic boundary-layer receptivity over a parabola in this example. It is helpful to understand the physical mechanisms of the transition process depending on the character of small environmental perturbations, which often causes boundary-layer instability, amplification, and interaction of different instability modes to laminar flow breakdown. After obtaining the steady solution, we impose perturbations to the basic flow in the freestream. The freestream is $M_\infty = 15$, $T^*_\infty = 192.989K$, $Re_\infty = 6026.55$, and the perturbations are $[u', v', p', \rho']^T_\infty = [|u'|, |v'|, |p'|, |\rho'|]^T_\infty e^{\mathrm{Im}k[x-(1+M_\infty^{-1})t]}$. Figure 7 shows the contours of the instantaneous velocity perturbation v', the Fourier amplitude, and the phase angle after the unsteady flow has been computed for 30 period time. The v' contours indicate the instability waves developing in the boundary layer because of the dominant instability waves near the surface. It is also seen very clearly in the Fourier amplitude and phase angle contours that two instability waves, named the first mode wave and the second mode wave, respectively, are generated. On the surface, the first mode is generated near the leading edge ($x < 0.2$), whereas the second mode is generated downstream. Figure 8 shows the solutions [15] by Zhong with his fifth-order linear scheme for the same test. Zhong's wave fields provide the region between the bow shock and the body surface. However our results provide a larger region where there is a bit of oscillation behind the bow shock. After comparing the wave structures between the bow shock and the surface, especially in the boundary layer, we know the solutions by Zhong's scheme and our WCNS-E-5 are well conformed to each other.

From the instantaneous entropy perturbation distributions in Fig. 9, we can see that the decay of the first mode wave and the growth of the second mode wave at about $x = 0.2$ are divided by a sudden change on the surface. The perturbation changes dramatically between the two modes. The change points captured by Zhong's scheme and ours are almost at the same location.

V. Conclusions

The Fourier analysis and applications of WCNS are studied to show their high-order characteristics. By the Fourier analysis, the features of WCNS, in contrast with EUW-5 and Padé schemes, are discussed in terms of dissipative and dispersive errors, the resolving

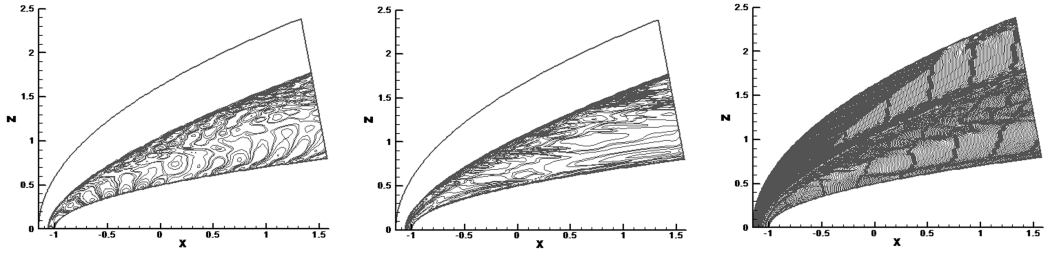

a) b) c)

Fig. 7 Unsteady contours by WCNS-E-5: a) instantaneous velocity, b) Fourier amplitude, and c) Fourier phase angle.

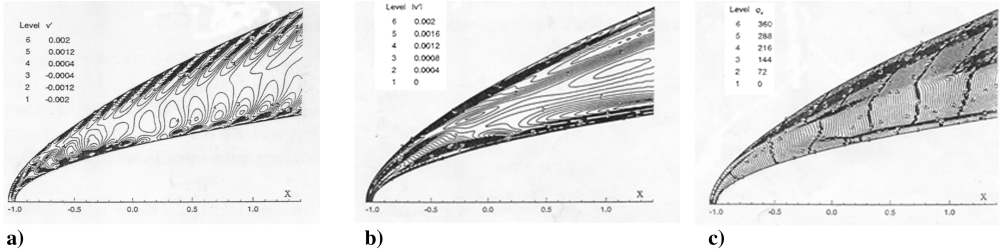

a) b) c)

Fig. 8 Unsteady contours by Zhong's explicit fifth-order shock-fitting upwind scheme [15]: a) instantaneous velocity, b) Fourier amplitude, and c) Fourier phase angle.

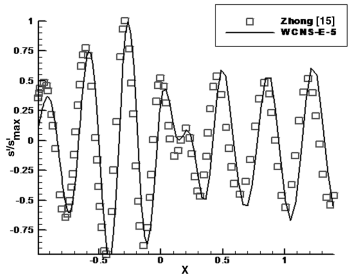

Fig. 9 Instantaneous entropy on surface.

efficiency and the multidimensional phase-speed anisotropy in the smooth region. The analytical results show that WCNS have better characteristics than EUW-5 in the parasite errors and they also seem more resolving efficient than EUW-5 and Padé. It may be seen that for the high-order schemes, the difference of anisotropic errors is little among one another, and they are altogether limited to a narrow range of short waves.

The interpolations of variables at cell-edges are the dominant factor for the accuracy of WCNS, which is of fifth-order accuracy in the smooth region and third-order accuracy in the vicinity of discontinuities. Besides its behavior similar to WCNS-5, WCNS-E-5 is more efficient because of nontridiagonal inversion. After computing several multidimensional Euler and Navier–Stokes equations, WCNS-E-5 shows that it captures discontinuities robustly. Owing to the quite low numerical error, WCNS-E-5 differentiates the flow structure clearly and accurately. Moreover, WCNS-E-5 needs fewer grids and obtains less unphysical oscillation nearby the shock than some high-order WENO schemes.

Acknowledgments

This study was supported by China National Natural Science Foundation (No. 10225208 and No. 10321002). The first author thanks Zhang Hanxin for his very helpful advice.

References

[1] Lele, S., "Compact Finite Difference Schemes with Spectral-Like Resolution," *Journal of Computational Physics*, Vol. 103, No. 1, 1992, pp. 16–42.

[2] Gaitonde, D., and Shang, J. S., "Optimized Compact-Difference-Based Finite Volume Schemes For Linear Wave Phenomena," *Journal of Computational Physics*, Vol. 138, No. 2, 1997, pp. 617–643.

[3] Cockburn, B., and Shu, C. W., "Nonlinearly Stable Compact Schemes for Shock Calculations," *SIAM Journal on Numerical Analysis*, Vol. 31, No. 3, 1994, pp. 607–630.

[4] Hu, G. Q., Fu, D. X., and Ma, Y. W., "Numerical Study of Sound Generated by Shock-Vortex Interactions," *Acta Mechanica Sinica*, Vol. 33, No. 6, 2001, pp. 721–728.

[5] Zhang, H. X., Li, Q., and Zhuang, F. G., "On the Construction of High Order Accuracy Difference Schemes," *ACTA Aerodynamica Sinica*, Vol. 16, No. 1, 1998, pp. 14–23.

[6] Levy, D., Puppo, G., and Russo, G., "Fourth Order Central WENO Scheme for Multi-Dimensional Hypersonic Systems of Conservation Laws," *SIAM Journal on Scientific Computing*, Vol. 24, No. 2, 2002, pp. 480–506.

[7] Shu, C. W., "Essentially Non-Oscillatory and Weighted Essentially Non-Schemes for Hyperbolic Conservation Laws," NASA CR-97-206253, 1997.

[8] Deng, X. G., Maekawa, H., and Shen, Q., "Class of High Order Dissipative Compact Schemes," AIAA Paper 96-1972, 1996.

[9] Deng, X. G., and Maekawa, H., "Uniform Fourth-Order Compact Scheme for Discontinuities Capturing," AIAA Paper 96-1974, 1996.

[10] Jiang, G., and Shu, C. W., "Efficient Implementation of Weighted ENO Schemes," *Journal of Computational Physics*, Vol. 126, No. 1, 1996, pp. 202–228.

[11] Deng, X. G., and Mao, M. L., "Weighted Compact High-Order Nonlinear Schemes for the Euler Equations," AIAA Paper 97-1941, 1997.

[12] Deng, X. G., and Zhang, H. X., "Developing High-Order Accurate Nonlinear Schemes," *Journal of Computational Physics*, Vol. 165, No. 1, 2000, pp. 22–44.

[13] Deng, X. G., "High-Order Accurate Dissipative Weighted Compact Nonlinear Schemes," *Science in China, Series A*, Vol. 31, No. 12, 2001, pp. 1104–1117.

[14] Rai, M. M., and Moin, P., "Direct Simulations of Turbulent Flow Using Finite-Difference Schemes," *Journal of Computational Physics*, Vol. 96, No. 1, 1991, pp. 15–53.

[15] Zhong X., "Direct Numerical Simulation of Hypersonic Boundary Layer Transition over Blunt Leading Edges, Part 2: Receptivity to Sound," AIAA Paper 97-0756, 1997.

[16] Gustaffson, B., "Convergence Rate for Difference Approximations to Mixed Initial Boundary Value Problems," *Mathematics of Computation*, Vol. 49, No. 2, 1975, pp. 396–406.

[17] Leer, B. V., Thomas, J. L., and Roe, P. L., "Comparison of Numerical Flux Formulas for the Euler and Navier–Stokes Equations," AIAA Paper 87-1104, 1987.

[18] Steger, J. L., and Warming, R. F., "Flux Vector Splitting of the Inviscid Gasdynamic Equations with Application to Finite-Difference Methods," *Journal of Computational Physics*, Vol. 40, No. 2, 1981, pp. 263–293.

[19] Shu, C. W., and Osher, S., "Efficient Implementation of Essentially Non-Oscillatory Shock-Capturing Schemes 2," *Journal of Computational Physics*, Vol. 77, No. 2, 1988, pp. 439–471.

Z. Wang
Associate Editor